

INVESTIGATION ON THE HIGH-EFFICIENCY PROPULSION MECHANISMS OF DUCK-WEBBED PADDLING FOR BIOINSPIRED AIRCRAFT APPLICATIONS

Shenshen Cao[1,2,3], Wenqing Yang[1,2,3*], Yugang Zhang[1,2,3*], Xiulai Xu[1,2,3]

[1] School of Aeronautics, Northwestern Polytechnical University, Xi'an 710072, China

[2] Shenzhen Research Institute of Northwestern Polytechnical University, Shenzhen 518057, China

[3] National Key Laboratory of Aircraft Configuration Design, Xi'an 710072, China

Abstract

Amphibious aerial-aquatic unmanned aerial vehicles (UAVs) possess promising prospects in cross-medium missions, and bionic duck webbing offers an effective route to high-efficiency underwater thruster design. A high-fidelity 3D bionic model of mallard webbed foot is built via CATIA with inherent asymmetry, interdigital concaves and curved membrane edges, avoiding the oversimplified flat-plate assumption widely adopted in previous numerical studies. Systematic CFD simulations using the SST k-ω turbulence model are performed to quantify the effects of flapping frequency, swing amplitude, bilateral phase difference and concave structure on hydrodynamic performance.Results reveal that thrust rises in a super-quadratic manner dominated by flapping frequency, while swing amplitude improves thrust mildly with a lower power exponent. Synchronous dual-foot oscillation generates the maximum average thrust and lift yet induces violent force fluctuation; a phase difference near 0.3T optimizes propulsion efficiency, raises force duty cycle and restrains lateral disturbance. Compared with the original concave model, the flat-plate counterpart improves average thrust by 11.6% and reduces lateral force by 84.4% with negligible lift drop, verifying that geometric simplification enhances propulsive capacity. Despite superior hydrodynamic efficiency of flat plates, moderately thick skeleton structures should be reserved in practical thruster design for structural integrity and multi-functionality. This study clarifies the biomechanical propulsion mechanism of natural duck paddling and provides theoretical guidance for parametric optimization of bionic webbed thrusters for amphibious UAVs.

Keywords: Numerical simulation, Webbed feet, Hydrodynamics, Propulsion

1. Introduction

Amphibious aerial-aquatic unmanned aerial vehicles (UAVs) feature outstanding environmental adaptability and have emerged as a cutting-edge research hotspot in recent years[1][2]. Combining the capability of aerial flight with underwater submergence, these drones can autonomously or controllably transition between air and water, perform diverse missions, and achieve a wider operational range, making them highly attractive. Waterbirds in nature exhibit remarkable multimodal cross-media locomotion capabilities, exemplified by cormorants[3][4], grebes[5], mallards[6], etc., providing excellent biomimetic inspiration for this field.

The webbed feet of waterbirds are a key functional structure enabling their multimodal cross-domain locomotion. Through this structure, waterbirds achieve efficient swimming and predation, multi-environment mobility, and energy savings. The webbed feet assist various locomotion modes, including surface swimming, underwater diving, surface takeoff, and landing. Dong et al.[7] and Huang et al.[8][9][10] found that webbed foot paddling can assist cormorants in rapid takeoff. Gough et al. discovered that the common eider employs two distinctive behaviors—"surface paddling" and "paddle-assisted flight"—to overcome hull speed limitations and achieve efficient surface escape[11]. Csillag and Ribak compared the underwater horizontal paddling kinematics and hydrodynamics of the common merganser and the common pochard, revealing evolutionary adaptive mechanisms for waterbird transition from surface to underwater locomotion[12]. Taylor-Burt and Biewener compared the hindlimb kinematics and in vivo lateral gastrocnemius muscle contractile function of mallards during vertical takeoff on land versus water, finding that mallards actively adjust hindlimb joint movement patterns and muscle contraction modes according to the mechanical properties of the different media (land vs. water)[6]. Aigeldinger and Fish, through video kinematic analysis, found that mallard ducklings rely on gait transition and dynamic lift to achieve surface skating, breaking through surface speed limitations[13]. Ribak et al. analyzed the hydrodynamic characteristics and energy expenditure of webbed foot paddling during bottom resting and foraging by the bufflehead, finding that continuous paddling counteracts buoyancy to achieve "hovering," with drag-based propulsion dominating[14]. Clifton and Biewener used 3D motion capture to analyze the swimming and turning kinematics of the common loon, clarifying that it relies on lift-based propulsion, controls speed by adjusting stroke duration, and uses combinations such as differential timing of webbed foot force generation and body roll for turning[15]. Furthermore, the paddling trajectory of waterbird webbed feet is not a simple reciprocating motion but a complex motion combining vortex generation, flexible deformation, and inertia utilization. For instance, Johansson and Norberg found that the propulsive force generated by webbed feet derives not only from hydrodynamic drag but also from hydrodynamic lift, with the webbed foot transitioning from drag-based to lift-based propulsion modes through vortex generation and shedding enabled by its triangular structure[16]. Additionally, waterbirds achieve precise steering by adjusting toe angles; biomimetic webbed feet can provide vector propulsion capabilities for drones, enhancing surface swimming, underwater hovering, reversing, and other maneuverability. Hydrodynamic research on webbed feet helps reveal the interaction mechanisms between paddling webbed feet and water, directly inspiring the biomimetic design of drone propulsors, and is essential for optimizing propulsion efficiency, underwater maneuverability, and stability of water-air amphibious drones.

Currently, most research on the function and hydrodynamic characteristics of webbed feet is based on kinematic observations and statistical methods, lacking quantitative results. The few studies based on computational fluid dynamics (CFD) also lack more precise simulation models, often employing simplified flat-plate foot models that neglect some morphological features. For example, Huang et al.[10] simplified the webbed foot as a flexible flat plate, while Xu et al.[17] and Liu et al.[18] further simplified it as a rhombic plane. However, the hydrodynamic characteristics of webbed feet are influenced not only by kinematic factors such as frequency, amplitude, and phase difference but also by morphological features such as asymmetry and interdigital indentations. Among current studies, only Huang et al.[19] fully considered the realistic geometry of the webbed foot, integrating skeleton skinning technology and CFD fluid-structure interaction simulation to construct an integrated numerical framework capable of reproducing skeletal motion and passive soft tissue deformation of cormorant webbed feet. However, their simulations focused on a single typical

turning posture, lacking comparative analysis under multiple operating conditions and motion modes, thus limiting the generalizability of their conclusions.

Therefore, this study takes the mallard's webbed foot as a biomimetic prototype. Based on biological morphological data, it overcomes the common flat-plate simplification in existing simulations. A simplified biomimetic duck webbed foot 3D model was constructed using CATIA software, fully retaining three key morphological features of the duck's webbed foot: asymmetry of the toe bone arrangement, interdigital indentation structure, and the curved outer edge of the webbing. This model achieves an advancement from geometric approximation to structural restoration, providing a reliable digital foundation for qualitatively and quantitatively revealing the form-function relationship. Combined with Pointwise mesh generation and ANSYS Fluent fluid simulation technology, using the SST k-omega turbulence model for hydrodynamic numerical simulation, we systematically investigated the influence of four key factors—paddling frequency, stroke amplitude, phase difference between bilateral feet, and webbed indentation structure—on the propulsive hydrodynamic characteristics of duck webbed feet. The study reveals the biomechanical mechanisms underlying the mallard's efficient and stable swimming, providing important theoretical basis and design references for the structural and kinematic parameter optimization of underwater biomimetic webbed-foot robots.

2. Materials and Methods

2.1 Geometric Model

Taking the webbed foot of mallard (Anas platyrhynchos) as the bionic prototype in this study, a three-dimensional bionic webbed foot model was established via CATIA software according to the anatomical and morphological parameters of mallard webbed feet published by Han et al.[20] The mallard webbed foot consists of tarsometatarsus, four phalanges (toe Ⅰ, Ⅱ, Ⅲ and Ⅳ) and interdigital webbing. The bones feature a hollow lightweight configuration, and the skeletal structure is illustrated in Figure 1. The interdigital webbing is a flexible thin membrane that passively expands or contracts following skeletal movements. The correlation between the dynamic mechanical characteristics of the tarsometatarsus and the joint angle of webbed toes is presented in Figure 2.

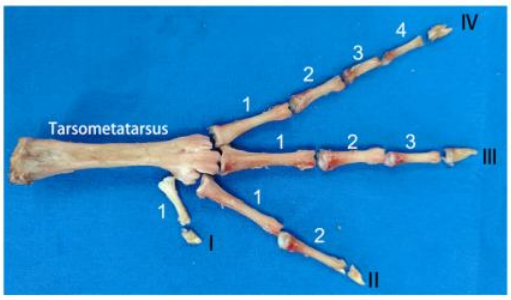


Figure 1 – Anatomical arrangement of the tarsometatarsus and phalanges[20].

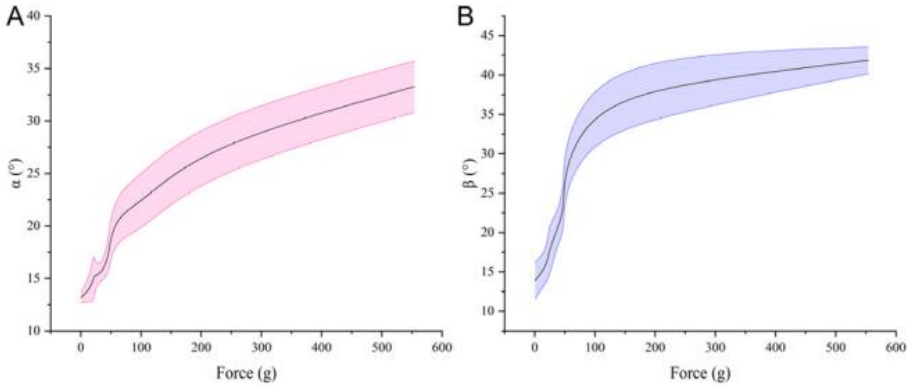


Figure 2 – Correlation between dynamic mechanical properties of tarsometatarsus and webbing joint angles. (A) α joint angle between the second and third toes; (B) β joint angle between the third and fourth toes.[20]

Key dimensions of the model strictly follow the measured data reported by Han et al.[20] To concentrate on hydrodynamic propulsion characteristics, the biological prototype is reasonably simplified to guarantee geometric similarity between the model and the original organism. The webbed foot model is shown in Figure 3. Tarsometatarsus, the first toe, as well as soft tissues such as skin, fat pads and tendons are neglected. The phalanges are simplified as variable-diameter rigid rods with the typical morphological feature of thick proximal ends and thin distal ends, and their primary dimensions are listed in Table 1. The interdigital webbing is modeled as a rigid membrane of uniform thickness while the curved edge profile of the webbing is retained. The α joint angle is 35°, the β joint angle is 40°, and the total area of the webbed foot model is 40 cm².

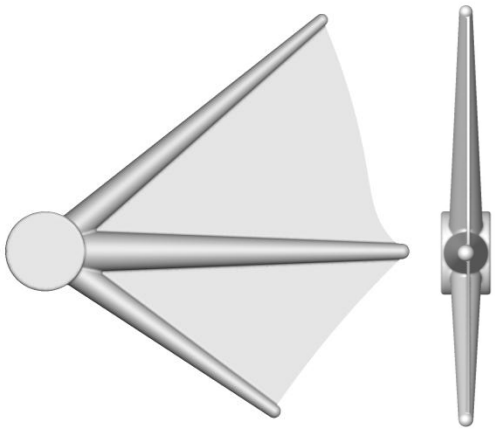


Figure 3 – The webbed foot model

Table 1 – Key dimensions of toes II, III and IV for the webbed foot model

	Otal length / mm	Proximal diameter / mm	Distal diameter / mm
Toe II	54	6.4	3
Toe III	71	9	3.4
Toe IV	72	6.9	2.7

2.2 Kinematic Simulation

In the present work, the motion of the webbed foot model is assumed to be composite rigid-body motion consisting of two independent Z-axis rotations centered at different pivotal points to replicate the real kinematics of a mallard webbed foot:

(1) Swing 1: The webbed foot undergoes simple harmonic rotation about the external fixed point O_1, simulating foot rotation around the knee joint:

$$\theta_1(t) = 0.5A\,sin\,(\omega t) \tag{1}$$

(2) Swing 2: The webbed foot performs complex periodic oscillation around point O2 on the model, representing rotational motion about the ankle joint:

$$\begin{aligned}\theta_2(t) = {} & 0.7611 - 0.6622\cos(\omega t) + 0.1919\sin(\omega t) - 0.2355\cos(2\omega t) + 0.2920\sin(2\omega t) \\ & + 0.04219\cos(3\omega t) + 0.1721\sin(3\omega t) + 0.09605\cos(4\omega t) + 0.01376\sin(4\omega t) \\ & + 0.03587\cos(5\omega t) - 0.04772\sin(5\omega t) - 0.01481\cos(6\omega t) - 0.03153\sin(6\omega t) \\ & - 0.0232\cos(7\omega t) - 0.002539\sin(7\omega t) - 0.009714\cos(8\omega t) + 0.01632\sin(8\omega t)\end{aligned} \tag{2}$$

Here, A denotes swing amplitude, $\omega=2\pi f$, where f is the flapping frequency of the webbed foot and t represents physical time. The spacing L_1 between O_1 and O_2 is 66 mm, consistent with the tarsometatarsal length measured by Han et al., as illustrated in Figure 4.

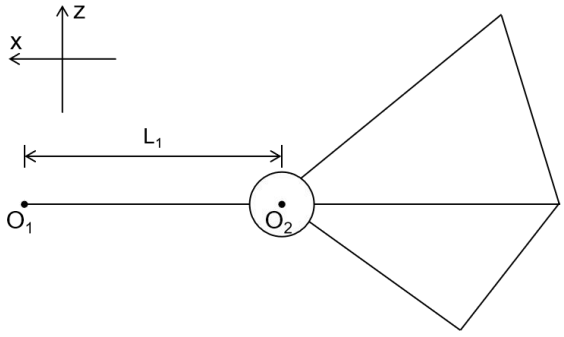


Figure 4 – Positional relationship between point O_1 and point O_2.

Taking f=1Hz and A=120° as an example, the kinematic pattern of the left webbed foot is presented in Figure 5.

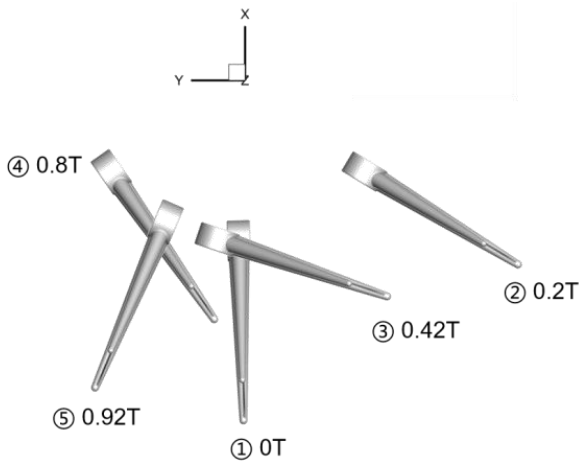


Figure 5 – Kinematic pattern of the left webbed foot.

For the dual-foot configuration, both webbed feet follow identical kinematic patterns as described above, differing only in initial motion timing. The right foot moves with a time delay relative to the left foot, introducing a phase difference of ΔT.

2.3 Mesh Model

Mesh generation was completed using Pointwise, and the computational domain was divided into the Background Domain and Component Domain. Both the single-foot and dual-foot computational domains correspond to a watery calculation zone with dimensions of 2000 mm (length) × 1000 mm (width) × 1000 mm (depth). The left webbed foot was defined as the wall boundary in the single-foot domain. Taking the dual-foot computational domain as an example (Figure 6): structured meshes were adopted for the background domain, with the inlet specified as velocity inlet boundary and the outlet set as pressure outlet boundary. Unstructured meshes were applied to the component domain, whose interfacing boundary with the background domain was defined as an interface boundary condition. The webbed foot surface was discretized with unstructured meshes and assigned to a no-slip wall boundary.

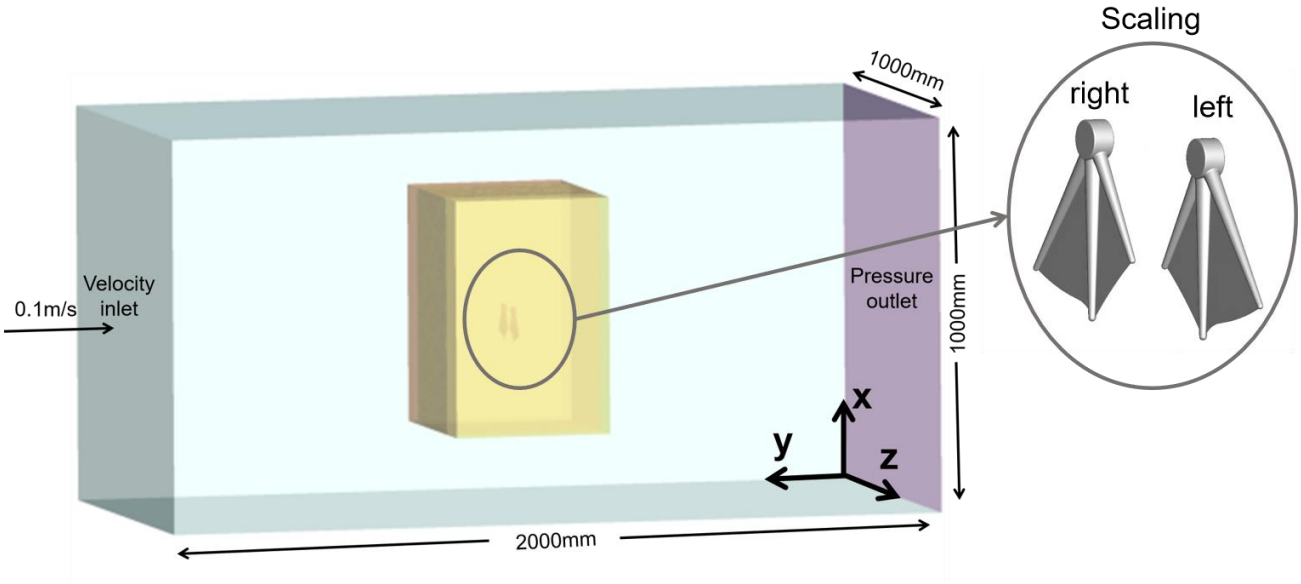


Figure 6 – Computational domain of the dual-foot model

Subsequently, the SST k-ω turbulence model was utilized in ANSYS Fluent to simulate the foot kinematics and calculate hydrodynamic performance. The incoming flow velocity was set to 0.1 m/s, and a mesh independence study was carried out for verification.

3. Results and Discussion

3.1 Effects of Frequency on Mechanical Characteristics

In this section, the left webbed foot is selected as the research object. Under identical initial setup and environmental parameters with a fixed swing amplitude of 120°, only the swing frequency is varied at seven levels: 0.5 Hz, 1 Hz, 2 Hz, 3 Hz, 4 Hz, 5 Hz and 6 Hz. Owing to the periodic motion of the webbed foot, the lift, thrust and lateral force all vary periodically, as illustrated in Figure 7 taking f=1Hz as an example. Compared with lift and thrust, the lateral force is negligible. Meanwhile, as illustrated in Figure 8, the vorticity visualization clearly reveals the trailing vortex shedding. This

intuitively verifies the conclusion proposed by Johansson and Norberg: the propulsion of webbed feet relies not merely on drag force; instead, their triangular geometry actively generates and harnesses edge vortices, enabling a transition from drag-dominated to lift-dominated propulsion[16].

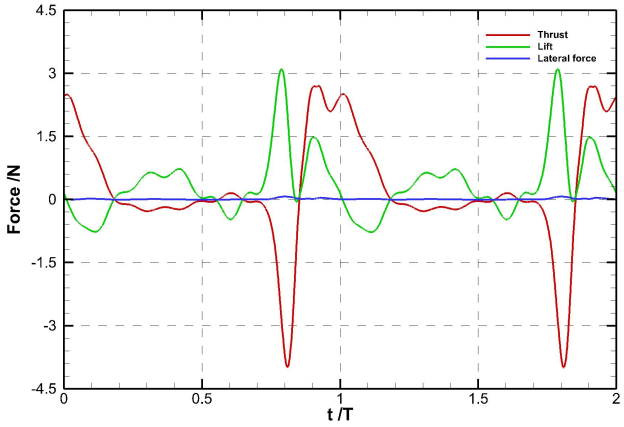


Figure 7 – Curves of thrust, lift and lateral force of the left webbed foot at *f*=1 Hz and *A*=120°.

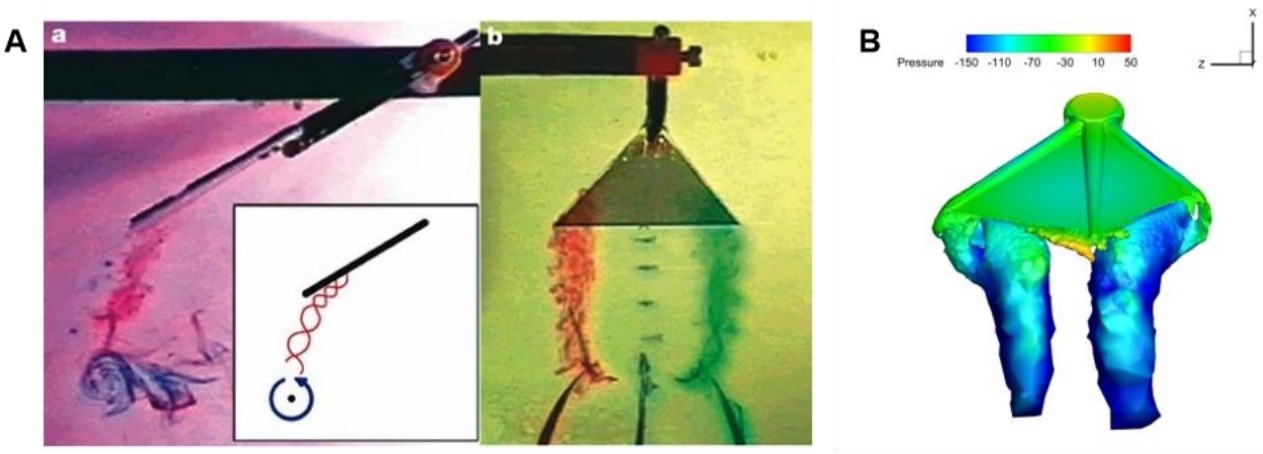


Figure 8 – Visualization of trailing vortices(A) The vortex shedding discovered by Johansson and Norberg[16];(B) The vortex shedding of left foot at *f*=1Hz,*A*=120°.

The time-averaged values of thrust, lift and lateral force within stable cycles at different frequencies were calculated, and the results are plotted in Figure 9. It is evident that both thrust and lift remain extremely low at *f*=0.5Hz, with the average thrust as low as 0.032N. This indicates that low-frequency flapping hardly generates effective propulsive force and explains why mallards adopt a relatively high flapping frequency during swimming.

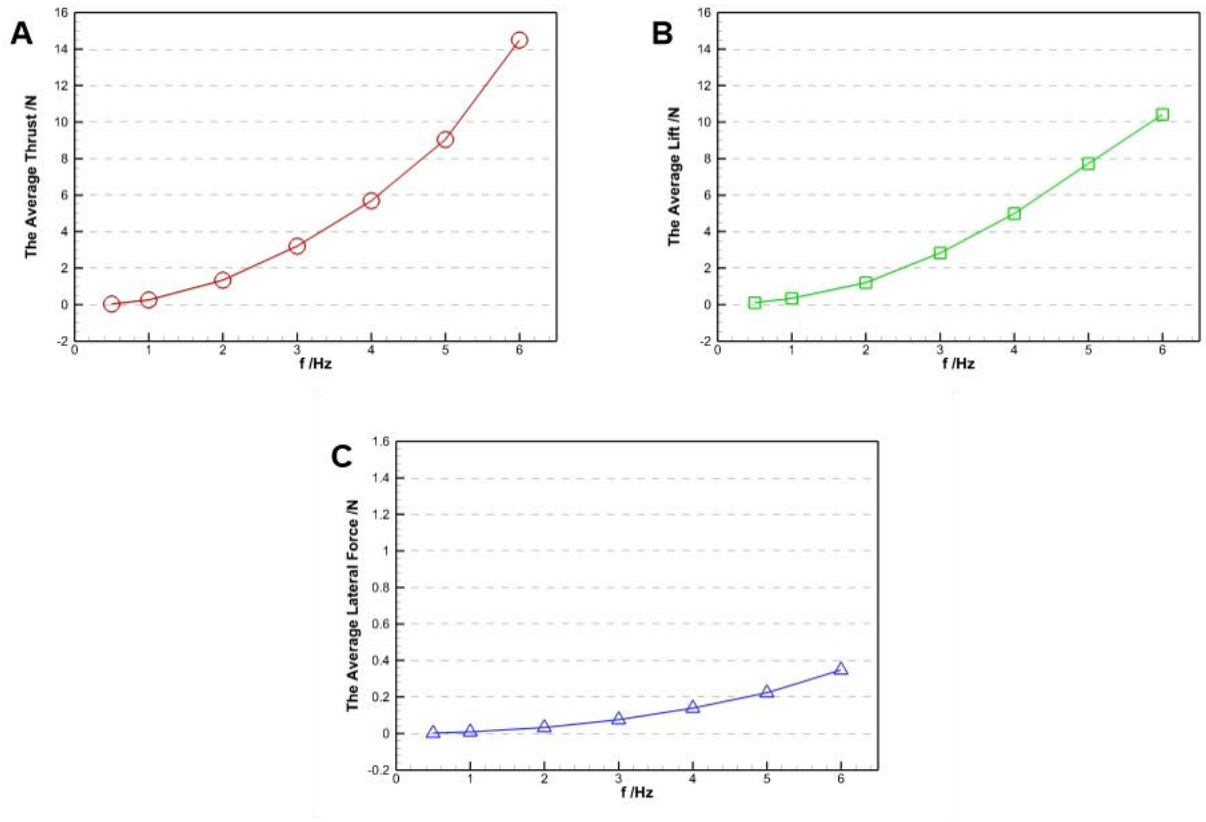


Figure 9 – Time-averaged thrust, lift and lateral force under various frequencies

Data fitting for the three groups of results was implemented via MATLAB to obtain the corresponding fitting formulas:

(1) Average thrust:

$$\overline{F_y} = 0.2256f^{2.312} + 0.1011 \tag{3}$$

(2) Average lift:

$$\overline{F_x} = 0.3957f^{1.836} - 0.07997 \tag{4}$$

(3) Average lateral force:

$$\overline{F_z} = 0.005387f^{2.316} + 0.003736 \tag{5}$$

The growth exponent of thrust with frequency is 2.312. The average thrust is merely 0.032 N at the low frequency of 0.5 Hz and rises to 14.49 N at 6 Hz, representing an over 450-fold increment that exceeds the conventional square law in fluid mechanics. By contrast, the growth exponent of lift is 1.836 with a much lower growth range, increasing from 0.105 N to 10.41 N, approximately a 99-fold rise. This demonstrates that lift is far less sensitive to swing frequency than thrust, revealing an essential discrepancy in the underlying mechanisms governing frequency effects on thrust and lift.

The superquadratic scaling of thrust with frequency originates from the enhancement of unsteady vortex-induced propulsion during webbed foot oscillation. At high frequencies, compact and stable attached vortices or vortex shedding systems form along the leading and trailing edges of the webbing. Such vortex structures create low-pressure regions and jet flows, greatly improving the momentum transport efficiency per oscillation cycle. By comparison, lift mainly consists of pressure-

difference lift and unsteady leading-edge vortex lift of the webbed foot. As frequency increases, the linear velocity at the webbing tip rises proportionally, accompanied by an increased Reynolds number and gradual development of leading-edge vortices; periodic trailing-edge vortex shedding contributes considerably to vortex lift, while pressure-difference lift grows simultaneously.From an energy viewpoint, thrust rises more than 450 times and lift around 99 times when frequency increases from 0.5 Hz to 6 Hz. This demonstrates that raising flapping frequency serves as an efficient strategy for urgent fast propulsion, such as escaping predators or swimming against currents.The power exponent of lateral force is 2.316, induced mainly by geometric asymmetry of the webbed foot model. Its nonlinear dependence on frequency is slightly stronger than that of thrust, yet its magnitude remains marginal: lateral force equals only 0.35 N at 6 Hz, less than 2.5% of the thrust at the same frequency.

3.2 Effects of Swing Amplitude on Mechanical Characteristics

In this set of simulations, the left webbed foot was still taken as the research subject with a fixed oscillation frequency of 1 Hz. Only the swing amplitude was adjusted to seven levels: 100°, 110°, 120°, 130°, 140°, 150° and 160°, while the initial setup and environmental parameters remained identical across all cases. Figure 10 presents the cycle-averaged thrust, lift and lateral force obtained under steady periodic conditions for each working condition.

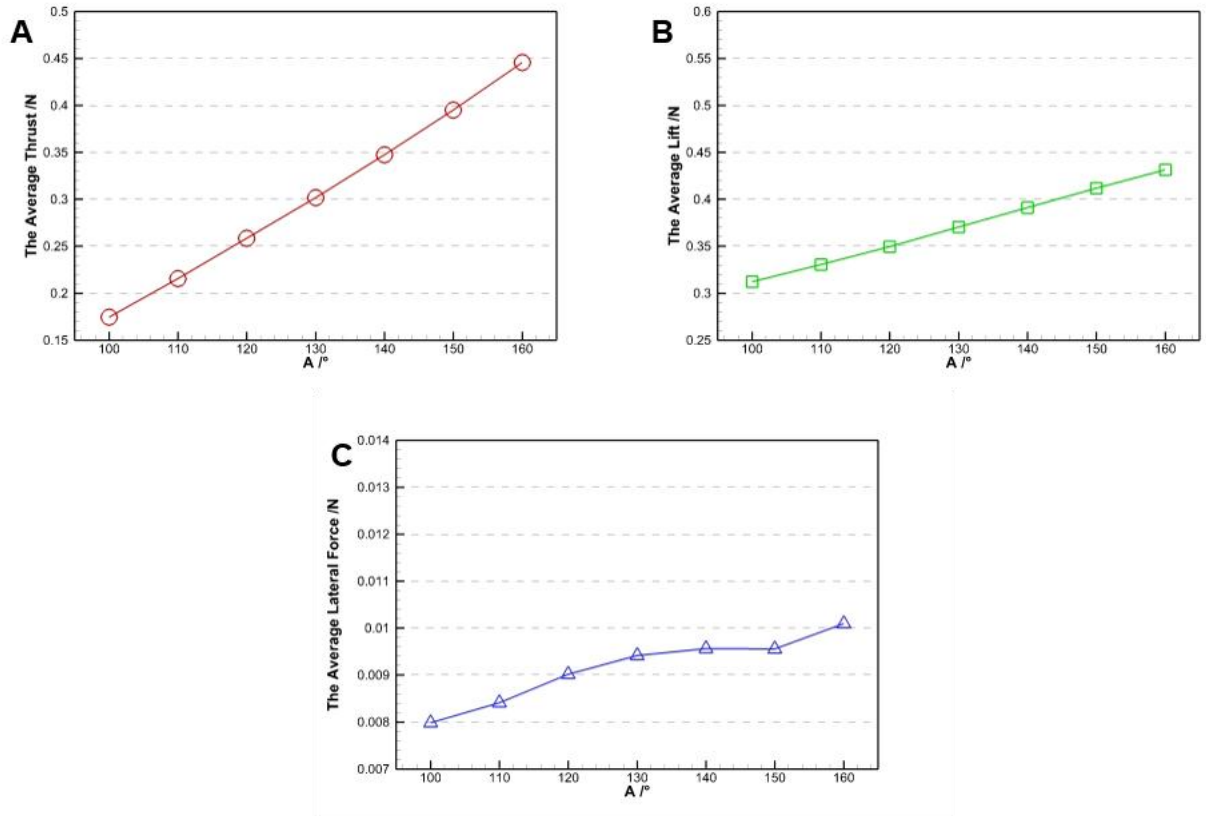


Figure 10 – Relationships between cycle-averaged thrust, lift, lateral force and flapping amplitude

The identical fitting method was adopted for the averaged thrust and lift data, and the fitted formulas are expressed as follows:

(1) Average thrust:

$$\overline{F_y} = 0.0002444A^{1.514} - 0.08569 \quad (6)$$

(2) Average lift:

$$\overline{F_x} = 0.0006118A^{1.206} + 0.1539 \quad (7)$$

The power-law exponent of thrust with respect to flapping amplitude is only 1.514. As the amplitude rises from 100° to 160°, thrust increases by approximately 2.65 times, far more slowly than the thrust growth driven by frequency variation. This indicates that flapping amplitude exerts a substantially weaker regulation effect on thrust compared with oscillation frequency. The underlying physical mechanism is as follows: increasing amplitude mainly extends the effective paddling stroke of the webbed foot. Nevertheless, restricted by water viscosity and the response speed of the surrounding flow field, the velocity gradient drops at the latter stage of the stroke, leading to diminishing increments of additional momentum.

The power exponent for lift against flapping amplitude is 1.206; lift rises by roughly 38.7% when the amplitude increases from 100° to 160°, also markedly lower than the lift growth induced by frequency change. This is because lift is predominantly governed by the projected area and normal velocity of the webbed foot, and amplitude expansion contributes much less to velocity improvement than frequency elevation.

Regarding lateral force, it first rises and then gradually saturates with growing amplitude, forming a gentle plateau within the range of 140°~150°, followed by a slight rebound at 160°. This behavior implies a potential self-stabilization effect of the webbed foot under large swing amplitudes: asymmetric flow induced by lateral perturbation is suppressed via the symmetrization mechanism of vortex structures. At excessively large swing angles, the tip of the rigid webbing approaches the ultimate rotational limit, accompanied by drastic distortion of instantaneous effective attack angle, severe local flow separation and abrupt vorticity surge on one side. The symmetry of bilateral vortex systems is completely destroyed, triggering a secondary rise in lateral force.

Although the absolute magnitude of lateral force remains much smaller than thrust and lift throughout all tested conditions, its saturation characteristic provides a design guideline: the amplitude range of 130°~150° yields the minimum growth rate of lateral force, which serves as the optimal swing range balancing high thrust and lift output against low lateral energy loss.

3.3 Analysis on Mechanical Characteristics of Phase Difference between Two Webbed Feet

In this group of simulations, paired left and right webbed feet were selected as research objects with fixed flapping frequency of 1Hz and swing amplitude of 120°. Only the phase difference of periodic motion between the two feet was adjusted to 0 T, 0.125 T, 0.25 T, 0.375 T and 0.5 T, while the initial setup and environmental parameters were kept consistent for all working conditions. The overall thrust and lift curves of paired feet under different phase differences are displayed in Figure 11. It can be observed that the peak values of total thrust and total lift gradually shift rightward with the increase of phase difference, which matches the kinematic characteristics of dual-foot motions.

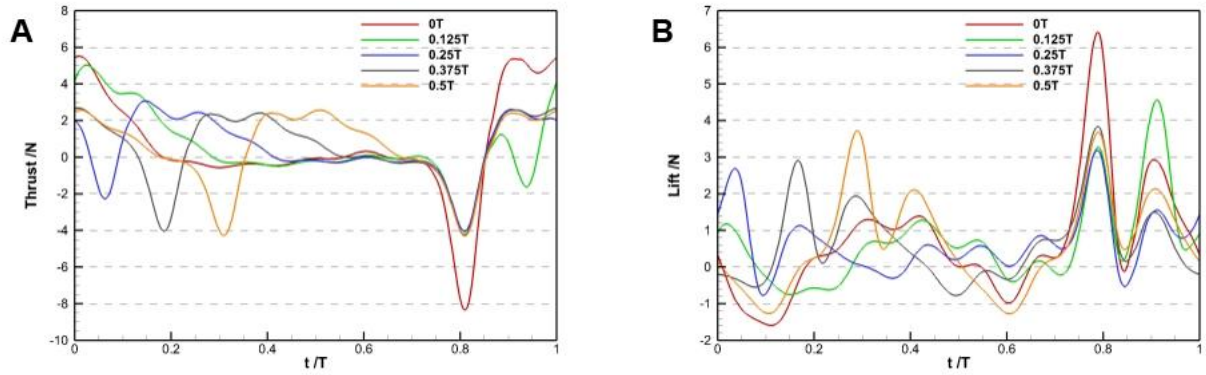


Figure 11 – Curves of total thrust and total lift of dual webbed feet

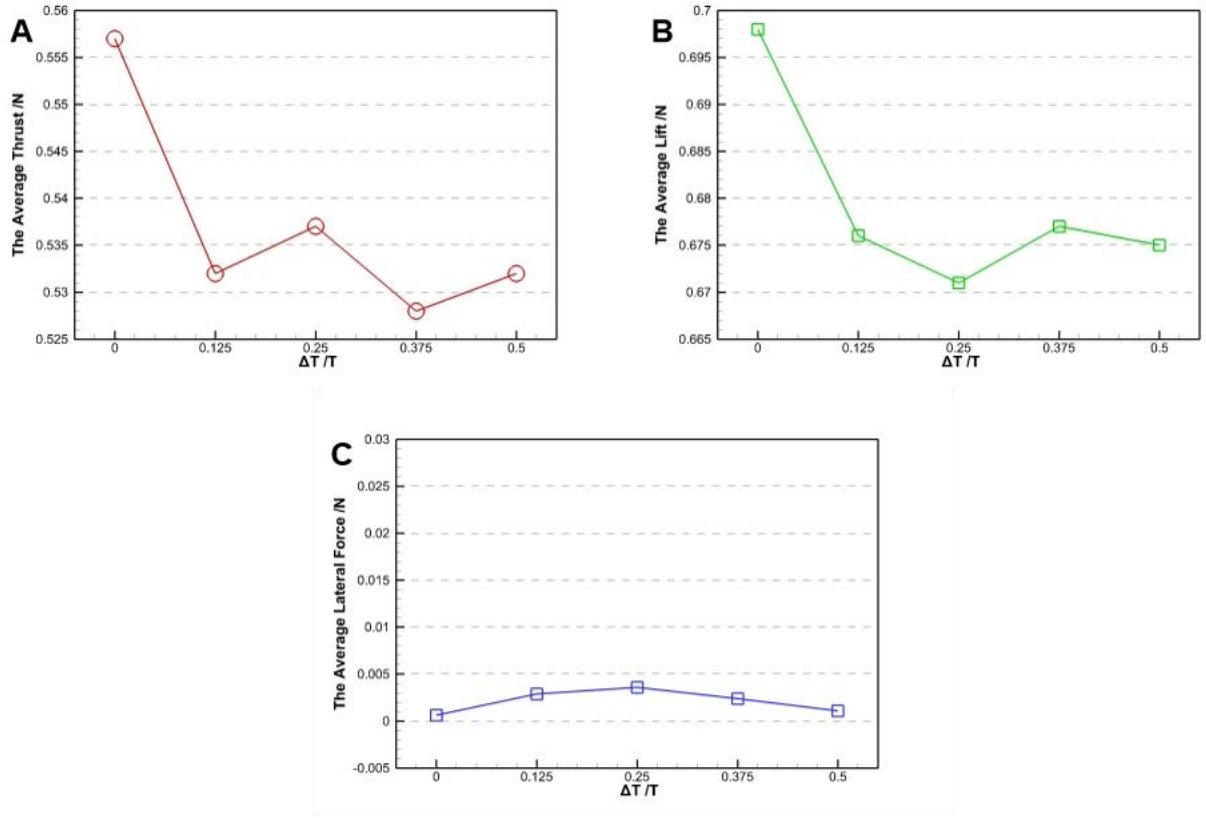


Figure 12 – Variation curves of cycle-averaged thrust, lift and lateral force against phase difference

The parametric study on phase difference reveals a critical design trade-off in dual-webbed-foot propulsion. As illustrated in Figure 12, synchronous flapping at zero phase difference (ΔT=0 T) yields the maximum cycle-averaged thrust (0.557 N) and lift (0.698 N). This arises from the full temporal superposition of peak thrust generated by the left and right webbed feet, leading to the maximum instantaneous resultant force.

This work further indicates that for asynchronous dual-foot motion, the average thrust decreases first, rises subsequently, and repeats such fluctuation as phase difference increases, with a local maximum occurring from 0.125 T to 0.375 T. Accordingly, the optimal phase difference for thrust production is approximately 0.3 T, rather than the 0.5 T anti-phase configuration widely adopted in

bionic robotic designs (Figure 12(A)). This finding agrees with the kinematic statistics reported by Hagar et al. for diving paddle locomotion of mandarin ducks (mean phase difference: 0.45 ± 0.043 T) and common pochards (mean phase difference: 0.26 ± 0.167 T). It suggests that aquatic birds have evolved similar asymmetric phase strategies over long-term natural selection, as an optimized compromise between propulsive efficiency and locomotion stability. Nevertheless, the introduction of phase difference induces moderate thrust loss, which can be attributed to mutual flow interference between the two webbed feet that degrades overall propulsion efficiency.

As shown in Figure 12(B), overall lift slightly drops with nonzero phase difference yet remains stable within 0.67–0.68 N with marginal discrepancies across all tested phase offsets, demonstrating that lift is less sensitive to phase variation than thrust.In terms of lateral force (Figure 12(C)), lateral loads nearly fully counteract one another under in-phase flapping (0.00062 N), and favorable cancellation is also achieved under anti-phase motion (0.0011 N). The lateral force peaks at 0.25 T (0.0036 N), yet this peak magnitude remains far lower than thrust and lift and exerts negligible adverse impacts on straight-line cruising performance.

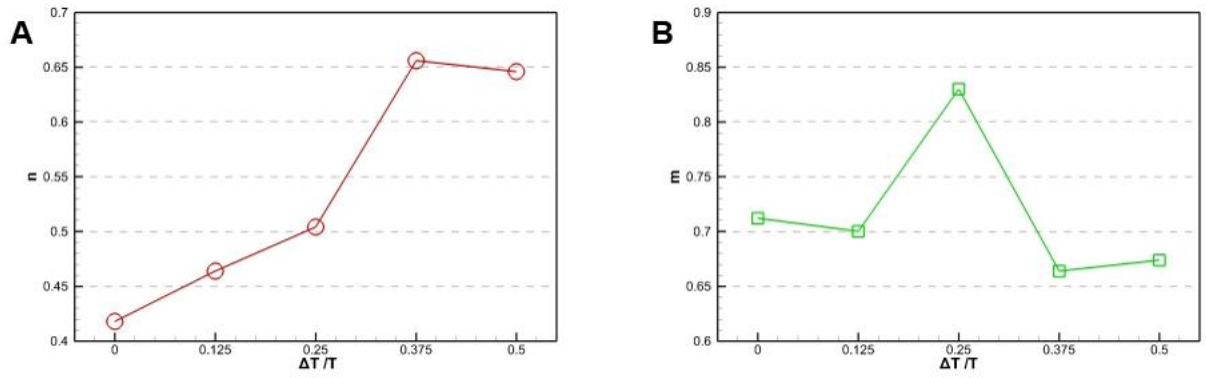


Figure 13 – Duty-cycle curves of positive thrust and positive lift

In the present study, the proportion of positive thrust and positive lift within one oscillation cycle is defined as the positive thrust duty cycle *n* and positive lift duty cycle *m*, respectively. Although in-phase flapping (ΔT=0 T) produces the maximum mean thrust, the corresponding positive thrust duty cycle is only 0.418. This indicates that thrust turns negative (i.e., drag force) for more than half of the full cycle, resulting in intense thrust pulsation, periodic fluctuation of duck body velocity and degraded cruising smoothness (Figure 13(A)).With the introduction of phase difference, the average thrust declines moderately, whereas the positive thrust duty cycle rises continuously and peaks at 0.656 at ΔT=0.375 T, followed by a slight drop to 0.646 at ΔT=0.5 T yet staying at a high level; accordingly, thrust pulsation is greatly suppressed. The underlying physical reason lies in the staggered timing of peak thrust from the two webbed feet: when one webbing is in the power stroke for propulsion, the other enters the retraction stroke, and its peak drag is offset in time, effectively filling the negative-thrust interval of the overall resultant force.As presented in Figure 13(B), the positive lift duty cycle reaches its maximum value of 0.830 at ΔT=0.25 T, meaning lift remains positive for nearly the entire cycle with optimum stability and minimum lift fluctuation.

Therefore, for engineering practice, in-phase flapping (ΔT=0 T) becomes the optimal option when maximum cruising speed is prioritized, as both average thrust and average lift attain their maxima at zero phase difference. Nevertheless, this scheme suffers from the lowest positive thrust duty cycle and severe thrust pulsation, which deteriorates locomotion stability. If smooth cruising is the primary

target, ΔT=0.375 T or ΔT=0.5 T is preferable: the thrust duty cycle increases remarkably with prolonged duration of positive thrust and steadier output, at the cost of a slight reduction in average thrust. When superior lift stability is specially required, ΔT=0.25 T serves as the best alternative, where the positive lift duty cycle hits 0.83 and lift fluctuates marginally with positive values over most of the stroke cycle.

3.4 Effects of Concave Cavity Structure

In this set of simulations, a flat-plate model with the identical membrane thickness as the original webbed foot was fabricated according to the projected outline of the baseline model, as shown in Figure 14(D). Under identical computational domain configuration, boundary conditions, kinematic law and other setup parameters, CFD simulations were performed to calculate hydrodynamic performance at a flapping frequency of 1 Hz and swing amplitude of 120°.Comparisons against the baseline model under identical operating conditions are plotted in Figure 14(A-C). The results demonstrate that the peak values of thrust and lift for the flat-plate model increase noticeably, while the lateral force presents an opposite trend accompanied by a smoother force curve.

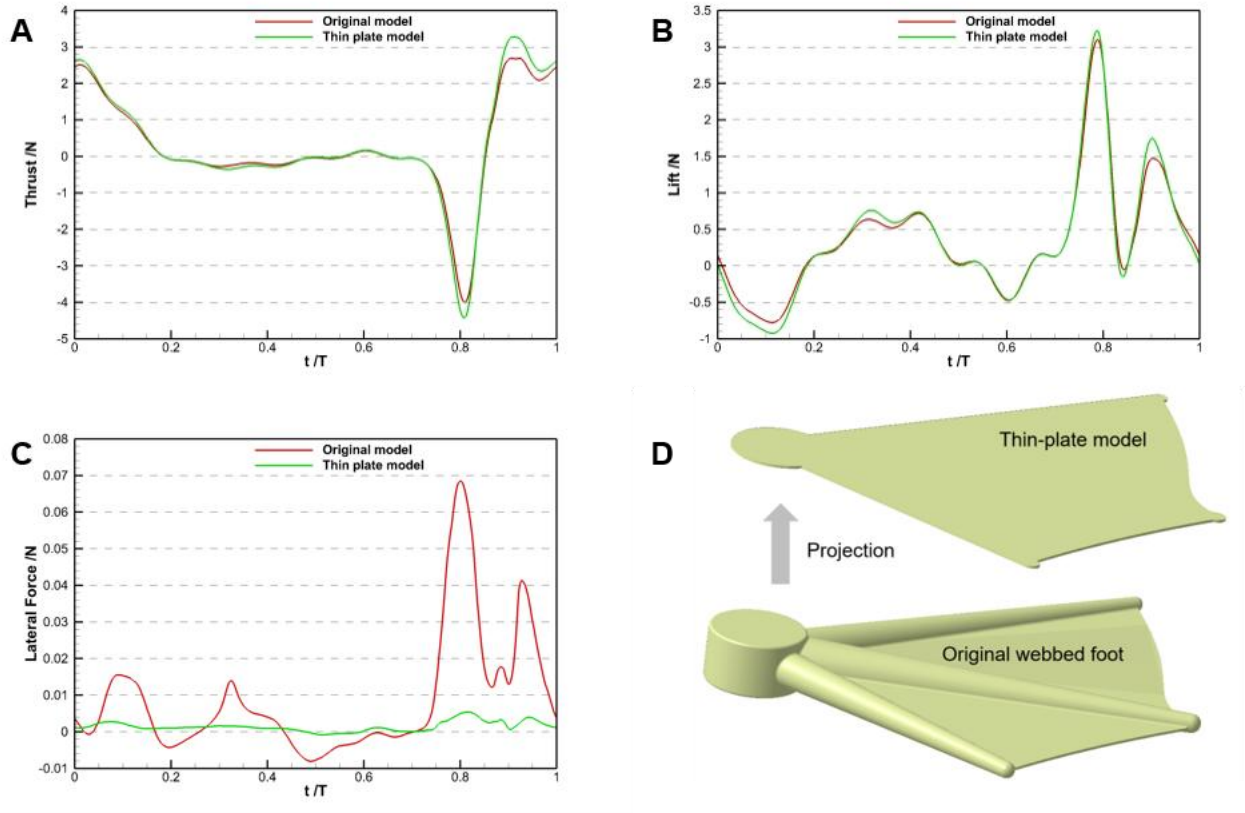


Figure 14 – Hydrodynamic force curves of the original model and flat-plate model under the condition of f=1 Hz and A=120°

Table 2 – Time-averaged forces of the baseline model and thin-plate model at f=1 Hz and A=120°

	Average thrust / N	Average lift / N	Average lateral force / N
Original model	0.258	0.349	0.0090
Thin plate model	0.288	0.345	0.0014
Growth rate	11.6%	-1.1%	-84.4%

Comparisons of hydrodynamic performances between the baseline and flat-plate models are

summarized in Table 2. The flat-plate model yields an 11.6% increment in cycle-averaged thrust and an 84.4% reduction in lateral force, while lift remains nearly unchanged with merely a 1.1% drop. Such results reveal that the flat-plate webbed configuration delivers prominent thrust augmentation and lateral force suppression.

This finding provides crucial guidance for bionic design. The physical mechanism responsible for thrust improvement is interpreted as follows: the baseline model features varied thickness and curved surfaces, which introduce extra pressure drag during oscillation. Besides, the bulky toe geometry disturbs concentrated trailing vortex shedding and disperses vortex structures, deteriorating the efficiency of momentum exchange. In contrast, the flat-plate model has uniform thickness and smooth planar surfaces, facilitating regular trailing vortex generation with higher vortex strength and stable shedding frequency, which strengthens jet-induced thrust. Lift is almost identical for the two configurations because lift is dominated by the normal fluid force, strongly correlated with projected area and effective attack angle. Identical projected outlines between the two models lead to similar normal loading, and the minor lift discrepancy originates from experimental random errors or localized pressure fluctuations induced by the curved geometry of the baseline model. The drastic reduction of lateral force arises from the elimination of asymmetric crossflow triggered by the three-dimensional contour of the baseline, hence realizing more symmetric flow on both sides of the flat plate.

Despite superior thrust performance of the flat-plate model, the inherent thickness variation and flexibility of natural duck webbing bring unique biological merits. First, tailored flexural stiffness enables optimized elastic energy storage and recovery analogous to energy recycling in biological tendons. Second, the curved profile improves maneuverability under low-speed incoming flow or complicated turbulent surroundings. Third, natural webbed membranes are equipped with tactile sensors to perceive flow orientation. Accordingly, a compromise between thickness layout and flexibility is required for bionic robot foot design to balance cruising stability and mechanical durability under complex operating conditions. Moreover, the marginal magnitude of lateral force (only 3.5% of thrust even for the baseline model) indicates that lateral disturbance is negligible for both solid and thin-plate webbed feet; therefore, design optimization should prioritize thrust and lift improvement.

4. Conclusions

Taking the webbed foot of mallard (Anas platyrhynchos) as the bionic prototype, this work systematically investigates the influences of flapping frequency, flapping amplitude, bilateral phase difference and concave membrane structure on the hydrodynamic propulsion performance of duck webbing, and clarifies the biomechanical mechanisms underlying the efficient and stable paddling of natural duck feet.

Flapping frequency serves as the dominant parameter for boosting propulsive thrust. By contrast, flapping amplitude contributes limited performance improvement and tends to increase joint load. Tests on dual-foot phase difference reveal the inherent trade-off between propulsion efficiency and cruising stability. In-phase flapping enables superposition of peak forces to maximize average thrust and lift, yet suffers from low thrust duty cycle, intense force pulsation and poor cruising smoothness. Introducing phase difference staggers the thrust and drag intervals of the two feet, increases force duty cycle and effectively suppresses kinematic fluctuation. Such asymmetric phase characteristics conform to the locomotion patterns of aquatic birds in nature; furthermore, appropriate phase offset

counteracts lateral force to guarantee stable forward navigation.

In addition, the flat-plate webbed configuration outperforms the original curved model in overall hydrodynamic performance. During biological evolution, natural duck webbing evolves to fulfill multiple non-propulsive functions including terrestrial weight bearing, gripping uneven muddy ground and flexural deformation for fluid wrapping. These functional constraints make natural webbing deviate from the geometric configuration for optimal pure thrust generation. By removing redundant features irrelevant to propulsion, the flat plate with identical outer outline achieves superior thrust output, demonstrating that geometric simplification outperforms full biological replication in bionic design. The optimum propulsion geometry is not a complete duplication of biological morphology but a simplified configuration retaining the primary contour while eliminating redundant structural features. Nevertheless, flat-plate structures suffer from insufficient structural strength and stiffness and cannot satisfy practical requirements of bionic webbed propulsors. Accordingly, bionic foot design should retain moderate curved thickness to improve structural stability and durability while approximating the hydrodynamic advantages of thin-plate geometry as much as possible.

In summary, this study quantifies the correlations between structural/motion parameters and hydrodynamic characteristics of bionic duck webbing, and establishes core design principles: frequency dominates thrust generation, amplitude plays an auxiliary tuning role, phase difference regulates cruising stability, and thin-plate geometry improves propulsion efficiency. The findings illustrate the evolutionary adaptation advantages of biological webbed feet and provide solid theoretical basis and engineering references for structural optimization and kinematic parameter matching of high-performance underwater bionic webbed propulsors.

5. Contact Author Email Address

The contact authors: Yang Wenqing, mailto: yangwenqing@nwpu.edu.cn; Zhang Yugang, mailto: zhangyugang@nwpu.edu.cn

6. Copyright Statement

The authors confirm that they, and/or their company or organization, hold copyright on all of the original material included in this paper. The authors also confirm that they have obtained permission, from the copyright holder of any third party material included in this paper, to publish it as part of their paper. The authors confirm that they give permission, or have obtained permission from the copyright holder of this paper, for the publication and distribution of this paper as part of the ICAS proceedings or as individual off-prints from the proceedings.

References

[1] Zeng, Z., Lyu, C., Bi, Y., et al. Review of hybrid aerial underwater vehicle: cross-domain mobility and transitions control[J]. *Ocean Engineering*, 2022, 248. DOI:10.1016/j.oceaneng.2022.110840.

[2] Yao, G., Li, Y., Zhang, H., et al. Review of hybrid aquatic-aerial vehicle (HAAV): classifications, current status, applications, challenges and technology perspectives[J]. *Progress in Aerospace Sciences*, 2023, 139. DOI:10.1016/j.paerosci.2023.100902.

[3] Xue, X., Zhao, X., Huang, J., et al. Experiments and analysis of cormorants' density, wing loading and webbed feet loading[C].//*IEEE International Conference on Robotics and Biomimetics (IEEE ROBIO)*. 2016:83-87.

[4] Huang, J., Gong, X., Wang, Z., et al. The kinematics analysis of webbed feet during cormorants' swimming[C].//*IEEE International Conference on Robotics and Biomimetics (IEEE ROBIO)*. 2016:301-306.

[5] Clifton, G. T., Hedrick, T. L., Biewener, A. A. Western and clark's grebes use novel strategies for running on

water[J]. *The Journal of Experimental Biology*, 2015, 218(8):1235-1243. DOI:10.1242/jeb.118745.

[6] Taylor-Burt, K. R., Biewener, A. A. Aquatic and terrestrial takeoffs require different hindlimb kinematics and muscle function in mallard ducks[J]. *The Journal of Experimental Biology*, 2020, 223(16). DOI:10.1242/jeb.223743.

[7] Dong, Y., Liang, J., Yang, X., et al. Modeling and simulation of cormorant's webbed-feet assisted take-off from water surface[C].//*IEEE International Conference on Robotics and Biomimetics (ROBIO)*. 2017:1659-1664.

[8] Huang, J., Li, J., Chen, H., et al. Design and CFD based simulation analysis of a biotic webbed feet propulsion mechanism for hydroplaning[C].//*IEEE International Conference on Robotics and Biomimetics (ROBIO)*. 2018:83-87.

[9] Huang, J., Wang, T., Lueth, T. C., et al. CFD based investigation on the hydroplaning mechanism of a cormorant's webbed foot propulsion[J]. *IEEE Access*, 2020, 8:31551-31561. DOI:10.1109/ACCESS.2020.2973356.

[10]Huang, J., Sun, Y., Wang, T., et al. Fluid-structure interaction hydrodynamics analysis on a deformed bionic flipper with non-uniformly distributed stiffness[J]. *IEEE Robotics and Automation Letters*, 2020, 5(3):4657-4662. DOI:10.1109/LRA.2020.3003774.

[11]Gough, W. T., Farina, S. C., Fish, F. E. Aquatic burst locomotion by hydroplaning and paddling in common eiders (Somateria mollissima)[J]. *The Journal of Experimental Biology*, 2015, 218(11):1632-1638. DOI:10.1242/jeb.114140.

[12]Csillag, H., Ribak, G. Underwater paddling kinematics and hydrodynamics in a surface swimming duck versus a diving duck[J]. *The Journal of Experimental Biology*, 2025, 228(9). DOI:10.1242/jeb.249274.

[13]Aigeldinger, Fish. Hydroplaning by ducklings: overcoming limitations to swimming at the water surface[J]. *J Exp Biol*, 1995, 198(7):1567-1574.

[14]Ribak, G., Swallow, J. G., Jones, D. R. Drag-based 'hovering' in ducks: the hydrodynamics and energetic cost of bottom feeding[J]. *PLOS One*, 2010, 5(9):1-11. DOI:10.1371/journal.pone.0012565.

[15]Clifton, G. T., Biewener, A. A. Foot-propelled swimming kinematics and turning strategies in common loons[J]. *The Journal of Experimental Biology*, 2018, 221(19). DOI:10.1242/jeb.168831.

[16]Johansson, L. C., Norberg, R. Å. Delta-wing function of webbed feet gives hydrodynamic lift for swimming propulsion in birds[J]. *Nature*, 2003, 424(6944):65-68. DOI:10.1038/nature01695.

[17]Xu, Y., Lin, X., Zhang, S., et al. Correlation analysis between waterfowl swimming behavior and propulsion efficiency[C].//*21st IEEE International Conference on Mechatronics and Automation (IEEE ICMA)*. 2024:1801-1806.

[18]Liu, L., Yu, Z.J., Chang, Z.Y. Hydrodynamic Analysis of Biomimetic Swimming Duck Flippers [J]. *Electromechanical Equipment* (in Chinese), 2015, 32(4):32-36. DOI:10.16443/j.cnki.31-1420.2015.04.008.

[19]Huang, J., Wang, T., Liang, J., et al. Biorobotic waterfowl flipper with skeletal skins in a computational framework: kinematic conformation and hydrodynamic analysis[J]. *Advanced Intelligent Systems*, 2023, 5(5). DOI:10.1002/aisy.202200380.

[20]Han, D., Liu, H., Ren, L., et al. From the analysis of anatomy and locomotor function of biological foot systems to the design of bionic foot: an example of the webbed foot of the mallard[J]. *Biomimetics*, 2023, 8(8):592. DOI:10.3390/biomimetics8080592.